NANO LETTERS

Letter

pubs.acs.org/NanoLett

Differentiation of Surface and Bulk Conductivities in Topological Insulators via Four-Probe Spectroscopy

Corentin Durand,[†] X.-G. Zhang,[†,‡] Saban M. Hus,[†] Chuanxu Ma,[†] Michael A. McGuire,[§] Yang Xu,[∥] Helin Cao,[∥] Ireneusz Miotkowski,[∥] Yong P. Chen,[∥,⊥] and An-Ping Li*[,†]

[†]Center for Nanophase Materials Sciences, Oak Ridge National Laboratory, Oak Ridge, Tennessee 37831, United States

[‡]Department of Physics and the Quantum Theory Project, University of Florida, Gainesville, Florida 32611, United States

[§]Materials Science and Technology Division, Oak Ridge National Laboratory, Oak Ridge, Tennessee 37831, United States

[∥]Department of Physics and Astronomy, Purdue University, West Lafayette, Indiana 47907, United States

[⊥]Birck Nanotechnology Center and School of Electrical and Computer Engineering, Purdue University, West Lafayette, Indiana 47907, United States

ABSTRACT: We show a new method to differentiate conductivities from the surface states and the coexisting bulk states in topological insulators using a four-probe transport spectroscopy in a multiprobe scanning tunneling microscopy system. We derive a scaling relation of measured resistance with respect to varying interprobe spacing for two interconnected conduction channels to allow quantitative determination of conductivities from both channels. Using this method, we demonstrate the separation of 2D and 3D conduction in topological insulators by comparing the conductance scaling of Bi_2Se_3, Bi_2Te_2Se, and Sb-doped Bi_2Se_3 against a pure 2D conductance of graphene on SiC substrate. We also quantitatively show the effect of surface doping carriers on the 2D conductance enhancement in topological insulators. The method offers a means to understanding not just the topological insulators but also the 2D to 3D crossover of conductance in other complex systems.

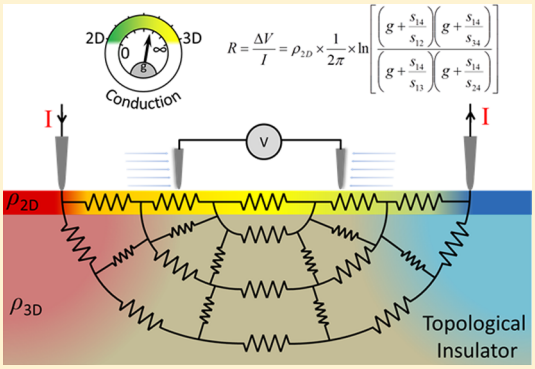

KEYWORDS: *Four-probe transport spectroscopy, topological insulator, electrical transport, dimensionality crossover, topological surface states, scanning tunneling microscopy*

Four-probe spectroscopy measurement with variable probe distances is the method of choice for studying materials where both surface and bulk contributions to electrical conduction are present. The common practice is to assume two decoupled conduction channels corresponding to the 2D conductance of surface states and the 3D conductance of bulk,[1−4] as schematically shown in Figure 1a, and deduce the dominant conduction mechanism through the dependence of the conductance with probe spacing. Such an assumption would only be valid if the potential profile across the surface were identical for both 2D and 3D conduction. However, the 2D and 3D conduction channels are usually coupled, with a conduction network that looks more like Figure 1b rather than Figure 1a, making it often difficult to cleanly decouple the two channels.

A recent example where both surface and bulk conductance can contribute to the electrical conductivity is topological insulators (TIs), a new state of matter with characteristic topological surface states and rich potentials for both fundamental physics and device applications. In TI materials, the existence of metallic surface states with massless Dirac dispersion and a simultaneous bulk insulating behavior is the hallmark of a TI state.[5,6] Indeed, the presence of TI states in Bi_2Te_3 and Bi_2Se_3 was confirmed from angle-resolved photoelectron spectroscopy (ARPES) experiments,[7−9] Shubnikov−de Haas oscillations[10−12] (SdHO), Aharonov−Bohm interference and weak antilocalization in magnetotransport,[13,14] as well as quasiparticle interference with scanning tunneling microscopy (STM).[15−17] Separating 2D conductivity from often unavoidable and more dominating 3D bulk contributions, however, has always been a challenge in transport experiments. This is due to the ubiquitous vacancies and antisite defects in the bulk, often rendering a result overwhelmed by the contribution of the bulk conductivity.

As a remedy for the leakage caused by the bulk states in Bi_2Te_3 and Bi_2Se_3, the ternary compound Bi_2Te_2Se has been used for studies of the surface transport because of its high bulk resistivity.[18] However, controlling the bulk conductivity is often made difficult, even for Bi_2Te_2Se, by unintentional doping from crystal defects.[18−20] Another way to address the problem is to use thin films[21,22] or nanoribbons[13] so that the surface to bulk ratio of the conduction contributions can be tuned by varying

Received: October 30, 2015
Revised: March 1, 2016
Published: March 8, 2016

DOI: 10.1021/acs.nanolett.5b04425
Nano Lett. 2016, 16, 2213−2220

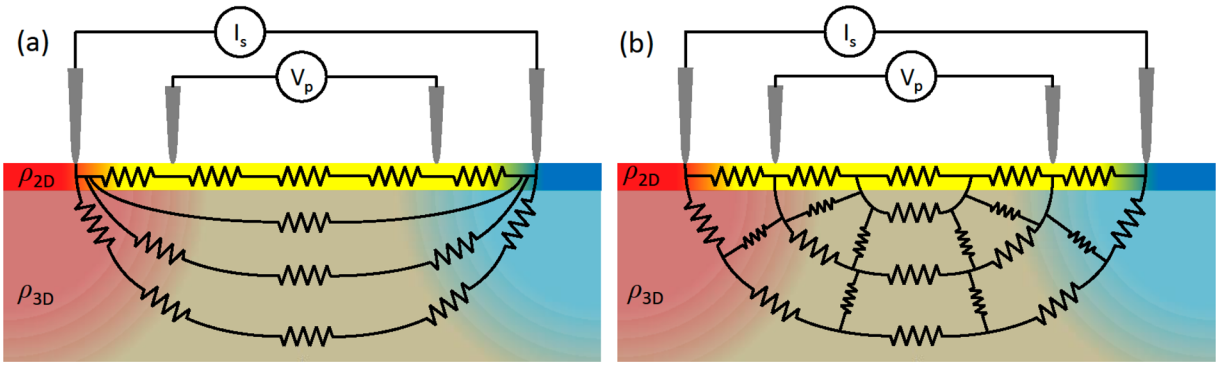

Figure 1. Schematic of four-probe transport measurement on a dual system made of a surface overlaying a semi-infinite bulk. (a) The two components (ρ_{2D} and ρ_{3D}) are represented as two decoupled parallel channels in a conventional model. (b) The system is represented by a generally inhomogeneous resistor network with leakage current paths at every point between the surface and the bulk.

the film or nanoribbon thickness. The measured conductance will still involve contributions from both the surface and bulk channels, although their relative ratio can vary from sample to sample.

Here we report a new method to account for both surface and bulk conduction mechanisms by solving the simultaneous current continuity equations for both 2D and 3D, allowing cross "channel" current at every point along the surface, as illustrated in Figure 1b. This enables the extraction of the conductivities from both conduction channels of a TI crystal based on a set of spectroscopy measurements using the four-probe scanning tunneling microscopy (STM).

In a four-probe spectroscopy setup schematically illustrated in Figure 1, two of the probes (source current probes) contacting the sample surface provide a current and the other two probes (voltage probes) measure the voltage drop over a selected sample area within which a current is established. In order to find an analytical expression where both 2D and 3D contributions to the transport (ρ_{2D} and ρ_{3D}) are taken into account, we first consider a surface of a solid with infinite thickness on which two current probes are separated by a distance s. At a point distance r away from the center of one of the probes and with $r \ll s$, the 2D current integrated over the circle is $I_{2D}(r)$. The total current $I = I_{2D} + I_{3D}$ integrated over the surface of a sphere of radius r is a constant. To derive a general expression for the potential, we first derive an expression for $I_{2D}(r)$ near $r \approx r_t$ in the polynomial form, with the probe radius being r_t, $I_{2D} = [a + b(r - r_t) + c(r - r_t)^2]I$. From this we can solve for the potential:

$$V_{2D}(r) - V_{2D}(r_t) = -I\int_{r_t}^{r}\frac{a + b(r - r_t) + c(r - r_t)^2}{2\pi r\sigma_{2D}}\mathrm{d}r$$
$$= -\left[(a - br_t + cr_t^2)(\ln r - \ln r_t) + (b - cr_t)(r - r_t) + \frac{1}{2}c(r - r_t)^2\right]\rho_{2D}\frac{I}{2\pi} \quad (1)$$

Note here the leading term for small r is $\ln r$, which means that the 2D current dominates close to the current probes. Rearrange to second order of $r-r_t$,

$$V_{2D}(r) - V_{2D}(r_t) = \left[\ln\left(\frac{1}{r} - \frac{b}{a + br_t}\right) - \ln\left(\frac{1}{r_t} - \frac{b}{a + br_t}\right)\right]\frac{a^2}{a + br_t}\rho_{2D}\frac{I}{2\pi} \quad (2)$$

Now it remains to find a set of equations for a and b. From the Ohm's law and $I = I_{2D} + I_{3D}$, integrating the 3D current over the surface of a sphere with radius r, we find,

$$-\frac{\mathrm{d}V_{2D}}{\mathrm{d}r} = -\frac{\mathrm{d}V_{3D}}{\mathrm{d}r} = \frac{I_{2D}}{2\pi r}\rho_{2D} = \frac{I - I_{2D}}{2\pi r^2}\rho_{3D} \quad (3)$$

Thus,

$$(\rho_{2D}r + \rho_{3D})[a + b(r - r_t) + c(r - r_t)^2] - \rho_{3D} = 0 \quad (4)$$

Solving this equation to the lowest orders of $r - r_t$, we find,

$$a = \frac{\rho_{3D}}{\rho_{2D}r_t + \rho_{3D}} \qquad b = -\frac{\rho_{2D}\rho_{3D}}{(\rho_{2D}r_t + \rho_{3D})^2}$$
$$c = \frac{\rho_{2D}^2\rho_{3D}}{(\rho_{2D}r_t + \rho_{3D})^3} \quad (5)$$

Suppose the two current probes are 1 and 4, and the two voltage probes are 2 and 3. Using the above result, and denoting $\vec{r}_1$ and $\vec{r}_4$ as the positions of the two current probes, we generalize eq 2 to all points on the surface including the effect of both current probes,

$$V(\vec{r}) = \left[\ln\left(\frac{\rho_{2D}}{\rho_{3D}} + \frac{1}{|\vec{r} - \vec{r}_1|}\right) - \ln\left(\frac{\rho_{2D}}{\rho_{3D}} + \frac{1}{|\vec{r} - \vec{r}_4|}\right)\right]\rho_{3D}\frac{I}{2\pi} \quad (6)$$

Because all factors involving r_t are canceled, there is no tip radius correction due to the current probes at all. The voltage probes may introduce a small error in the tip position due to its finite radius. This can be shown to be a high order term in r_t by averaging the above equation over a small circle of radius r_t. We use s_{ij} to represent the distances between the probes i and j. In a typical measurement, the penetration depth of the current distribution in the 3D bulk is roughly equal to the spacing between the current probes[23−26] (considering the sample thickness being much larger than the probe spacing). In order

DOI: 10.1021/acs.nanolett.5b04425
Nano Lett. 2016, 16, 2213−2220

to have a meaningful comparison between the 2D and 3D channels, we normalize the resistivity of the bulk ρ_{3D} and the distances s_{ij} by s_{14} and introduce a dimensionless parameter $g = (\rho_{2D}/\rho_{3D}) \times s_{14}$, which gives an estimate of the ratio between the contributions from the 2D surface and the 3D bulk to the total resistance. Then the measured resistance between probes 2 and 3 is given by,

$$R = \frac{\Delta V}{I} = \rho_{2D} \times \frac{1}{2\pi} \ln\left[\frac{\left(g + \frac{s_{14}}{s_{12}}\right)\left(g + \frac{s_{14}}{s_{34}}\right)}{\left(g + \frac{s_{14}}{s_{13}}\right)\left(g + \frac{s_{14}}{s_{24}}\right)}\right] \quad (7)$$

The expression given by eq 7 can be simplified for the 2D ($g \to 0$) limit,

$$R_{2D} = \rho_{2D} \times \frac{1}{2\pi} \ln\left(\frac{s_{24}s_{13}}{s_{12}s_{34}}\right) \quad (8)$$

and the 3D ($g \to \infty$) limit,

$$R_{3D} = \rho_{3D} \times \frac{1}{2\pi}\left(\frac{1}{s_{12}} + \frac{1}{s_{34}} - \frac{1}{s_{13}} - \frac{1}{s_{24}}\right) \quad (9)$$

These limits match the well-known formulas generally used for 2D and 3D conductance cases.[1,3,27] However, in the intermediate regime where both 2D and 3D currents are present, the total resistance cannot be calculated from a simple parallel resistor network formed with R_{2D} and R_{3D}. Rather it is given by eq 7.

In order to facilitate the fit of eq 7 to experiment, we define

$$X_g = \frac{1}{2\pi} \ln\left[\frac{\left(g + \frac{s_{14}}{s_{12}}\right)\left(g + \frac{s_{14}}{s_{34}}\right)}{\left(g + \frac{s_{14}}{s_{13}}\right)\left(g + \frac{s_{14}}{s_{24}}\right)}\right] \quad (10)$$

and for different values of g we plot R vs X_g parametrically through changing the distance between the voltage probes. The relationship between R and X_g is linear only for the correct value of g. The correct value of g is determined by tuning it until a linear plot is obtained. The slope of the plot gives ρ_{2D}, from which we then extract $\rho_{3D} = (\rho_{2D}/g)s_{14}$.

We first demonstrate the method using simulated resistance data generated from eq 7. For a test case, the four probes are perfectly aligned in a symmetric configuration, with a constant $\rho_{2D} = 2\pi\ \Omega$ and g ranging from 10^{-3} to 10^{6}. We add a random 5% fluctuation on the resistance values to simulate the uncertainty in experimental data. As shown in Figure 2, for $g < 0.1$ only ρ_{2D} can be determined accurately, while ρ_{3D} cannot be reliably extracted from the total resistance, indicating the dominance of 2D conduction. Conversely, for $g > 1000$, only ρ_{3D} can be determined, reflecting the dominance of 3D conduction. Within the range $0.1 < g < 1000$, both ρ_{2D} and ρ_{3D} can be extracted, with the error in the dominant conduction channel on the same level as the error of the total resistance, and the error in the minor conduction channel being significantly higher. The parameter windows for different conductance regimes may vary by changing the accuracy of measurement and by varying the probe spacing s_{14} as we discuss below.

The first key validation of the model is that it correctly identifies and quantifies purely 2D conduction. For this purpose we use experimental data measured on epitaxial graphene grown on an insulating substrate of SiC,[28−30] a well-documented 2D system[2]. The four-probe transport measurements are performed in a cryogenic four-probe STM under ultra high vacuum (UHV) environment (see Method for details).[27] On the surface, the four STM tips are arranged in a collinear configuration, with the distances s_{ij} between the probes as schematically shown in Figure 1. For a complete set of measurements, the voltage probes are moved step by step toward the center of the investigated area, while the positions of the outer source probes are fixed ($s_{14} \approx 38.6\ \mu$m in this case).

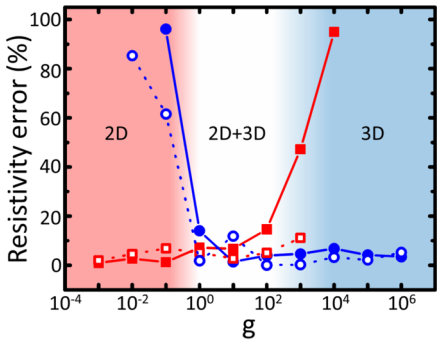

Figure 2. Relative error of the resistivities ρ_{2D} (red symbols) and ρ_{3D} (blue symbols) extracted from simulated data sets with constant s_{14} using eq 7. Open and closed symbols represent results from two different sets of probe positions. A random 5% fluctuation is added to the total resistance R before fitting to simulate the effect of measurement errors.

The measured resistance at $T = 82$ K with varying probe spacing is shown in Figure 3a. The best fit of the result using eq 7 gives $g = 0$, consistent with the expected 2D transport. Experimental data are represented by empty stars, and the red dotted line is the linear fit. Replotting the same data using $g = 5$, which if correct would contain a 3D component in the transport, yields a clearly nonlinear curve as shown in Figure 3b. Fitting with other finite values of g also yields nonlinear

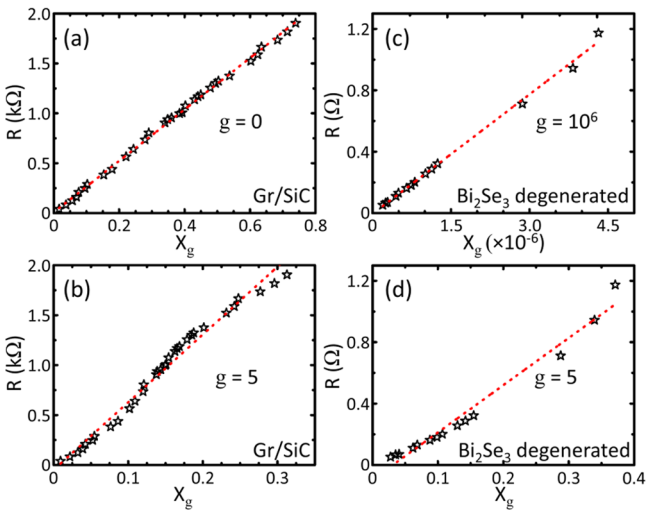

Figure 3. Four-probe transport measurements at $T = 82$ K for (a, b) graphene on SiC substrate and for (c, d) degenerated Bi_2Se_3. (a) Measured resistance R plotted as a function of the coefficient X_g with $g = 0$. (b) Plot of the graphene data with $g = 5$, for which a linear plot would imply a 3D contribution from the SiC substrate. (c) Measured resistance R plotted as a function of the coefficient X_g with $g = 10^6$ for a Bi_2Se_3 sample. (d) Plot of the Bi_2Se_3 data with $g = 5$, for which a linar plot would imply a 2D contribution from the surface.

DOI: 10.1021/acs.nanolett.5b04425
Nano Lett. 2016, 16, 2213−2220

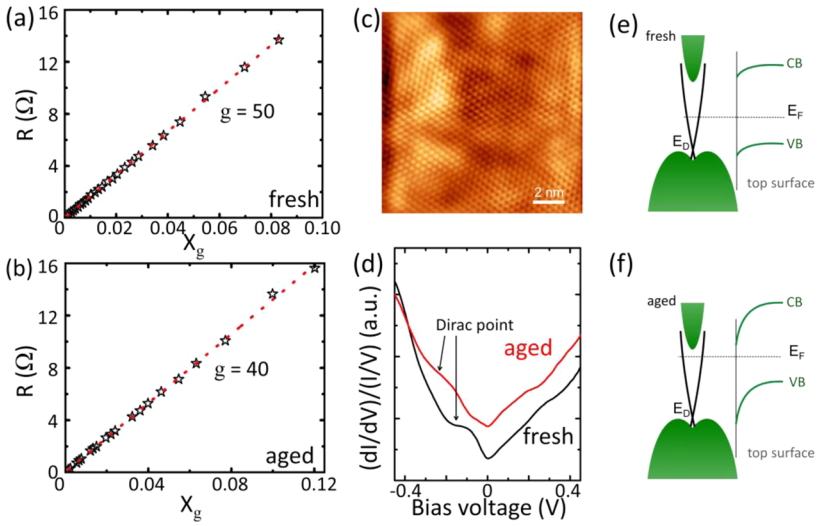

Figure 4. Four-probe transport measurements performed at T = 82 K on the "fresh" and the "aged" surfaces of Bi_2Te_2Se. (a) Mixed 3D and 2D transport with a linear R vs X_g at g = 50 in a freshly cleaved sample. (b) Enhanced 2D contribution with a linear R vs X_g at g = 40 after aging. (c) STM image with atomic resolution of the "fresh" Bi_2Te_2Se surface (V = −20 mV, I = 200 pA). (d) STS spectra of the same "fresh" (red spectrum, averaged over 385 curves) and "aged" (black spectra, averaged over 90 curves) surfaces. (e and f) Schematics of band bending in fresh and aged Bi_2Te_2Se, respectively.

curves. Thus, the system cannot be described as a mixed 2D and 3D system. From the slope in Figure 3a, we extract ρ_{2D} = 2579 Ω, consistent with previous studies on similar samples.[28]

To validate the 3D limit, we performed similar transport measurements (T = 82 K and with similar probe spacing s_{14}) on a cleaved Bi_2Se_3 surface. The measured resistance with varying probe spacing is plotted in Figure 3c. A linear fit with eq 7 is found for a factor g toward infinity (g = 10^6 is used here), indicative of the 3D nature of the transport. Using eq 7 with g ≥ 10^6, we extract a resistivity of ∼0.93 mΩ·cm for the bulk. In contrast, a linear fit cannot be obtained with a lower g value, as shown in Figure 3d with g = 5 (i.e., the ratio of 2D surface and 3D bulk resistance is 5). Thus, the system does not have a measurable 2D contribution to the transport, and the transport is dominated by the metallic bulk states. The same resistivity value can be extracted by using the 3D formula eq 9. Note that the 3D fit on the Bi_2Se_3 (shown in Figure 3c) does not necessarily rule out a contribution from topological surface to the electronic transport. That the extracted g is out of the detection window (higher than 10^3) places an upper limit of about 0.1% on a possible topological state contribution.

After validation in both the 2D and 3D limits, we employ this method to differentiate conductivities from the surface states and the coexisting bulk states in TI Bi_2Te_2Se. Like Bi_2Se_3, Bi_2Te_2Se has an ordered tetradymite structure, derived from Bi_2Te_3 by replacing the central Te layer with a Se layer. Because here the Se atoms are confined in the central layer the formation of Se vacancies and the antisite defects between Bi and Te atoms are expected to be less probable,[31] leading to much reduced bulk conductivity.[18,31] For transport measurement, we mechanically cleave Bi_2Te_2Se single crystals in the UHV chamber at room temperature and then characterize them at T = 82 K.

Figure 4a shows the resistance of Bi_2Te_2Se measured within 24 h post cleavage (denoted as fresh surface) and with a probe spacing s_{14} = 46.6 μm. The data can be best fitted with eq 7 using g = 50 ± 9, namely R_{2D}/R_{3D} ∼ 50 and only (2.0 ± 0.4)% of conductance is via the 2D channel. From this result, we extract ρ_{3D} = (15.35 ± 0.40) mΩ·cm and ρ_{2D} = (166 ± 25) Ω. The sample was then exposed to a residual pressure in the 1 × 10^{-9} Torr range (instead of the 2 × 10^{-10} Torr in normal operation) for 5 days (denoted as aged surface). We repeated the same measurement after the chamber is back to the normal pressure and the temperature is back at 82 K, care being taken to measure the same sample area. As shown in Figure 4b, we can see a slightly higher contribution from a 2D channel now, as the best fit to eq 7 is achieved with g = 40 ± 7, meaning that about (2.4 ± 0.4)% of the conductance comes from the 2D channel. On the aged sample, we extract ρ_{3D} = (14.81 ± 0.40) mΩ·cm and ρ_{2D} = (132 ± 20) Ω. Thus, the surface conductivity is enhanced by about 20.5% on the aged sample, while the bulk conductivity is enhanced only by about 3.5% as compared to the fresh sample. The relatively larger error bar of the 2D conductivity makes the enhancement of the surface conductivity less certain. However, the increased conductivity in the aged sample is much less likely to come from the bulk. In comparison, Analytis et al.[10] estimated the topological surface contribution to be around 0.1% of the conductance on Bi_2Se_3 at T = 1.4 K, Qu et al.[11] found a contribution around 0.3% on Bi_2Te_3 at T = 0.3 K, and the highest quantitative value of 6% was reported by Ren et al.[31] on Bi_2Te_2Se at T = 1.6 K.

To understand the difference between the fresh and aged Bi_2Te_2Se samples, we performed STM measurements to examine the structural and electronic properties of the surface under both conditions. Figure 4c shows a high-resolution STM image of the freshly cleaved surface, where the ordered triangular lattice is clearly resolved. The lattice constant is estimated to be 4.2 Å, consistent with the bulk value. The STM images taken on the aged surface show no obvious difference from those of fresh surface. However, a clear change in the local density of states (LDOS) is observed in scanning tunneling spectroscopy (STS) measurements that are performed on both surfaces in the same chamber and temperature as the transport measurements. Figure 4d shows the $(dI/dV)/(I/V)$ curves, each of which is averaged over multiple spectra to improve the statistics. On the fresh surface (black spectrum), the LDOS exhibits a characteristic V-shape near the Fermi level, with a clear dip at −0.15 V that can be assigned to the Dirac point of

DOI: 10.1021/acs.nanolett.5b04425
Nano Lett. 2016, 16, 2213−2220

the topological surface states. On the aged surface (red spectrum), the Dirac point shifts down to −0.24 V below the Fermi energy. The position of the Dirac point relative to the Fermi energy before and after aging is schematically illustrated in Figure 4e,f. For the fresh surface, at about 0.15 eV above the Dirac point the Fermi level is in the bulk band gap, consistent with the Shubnikov-de Haas oscillation measurement on similar samples.[32] After aging, at 0.24 eV above the Dirac point, the Fermi level moves closer to the bottom of the conduction band, indicating increased n-type doping. As a first order estimate of the doping, we convert these Dirac point values to charge-carrier concentration using the equation $n = E_D^2/\pi\hbar^2 v_F^2$, where $\hbar$ is the Planck's constant divided by 2π, n is the carrier concentration, and ν_F is the Fermi velocity ($\nu_F \sim 6 \times 10^5$ m/s).[33] The change of E_D from −0.15 V to −0.24 V yields an increase of n-type carriers from 4.6×10^{12} cm^{-2} of the fresh surface to 6.9×10^{12} cm^{-2} of the aged surface.

The gas doping effect on Bi_2Se_3/Bi_2Te_3 surfaces has been extensively studied,[34−36] and residual gases (H_2, CO, CO_2, and H_2O) in the UHV chamber are found to have an n-type doping effect on the surfaces of Bi_2Se_3 and Bi_2Te_3 after an extended period of exposure. While the doping effect increases the carrier density, the decrease in mobility due to doping is unlikely to cancel the effect. Consequently the conductance of the topological surface state increases with aging, explaining the observed 2D conductance enhancement in Figure 4b. Moreover, n-type doping leads to a downward band-bending, as depicted in Figure 4f. If the Fermi level moves above the bottom of the conduction band, a topologically trivial surface 2D electron gas will populate the triangular shaped quantum well. Such a quantum well state coexisting with the topological states further increases the 2D conductance on the aged surface. Indeed, a 2D contribution to the transport arising from additional carriers in opposition or in addition to the topological surface state has been reported in magnetotransport measurements on 3D TIs.[13,37,38]

As a comparison with Bi_2Te_2Se, we now study the conductance of Sb-doped Bi_2Se_3. For a lightly Sb-doped sample, bulk electrical resistivity (Figure 5a) measured with a quantum design physical property measurement system exhibits a dopant activation temperature around 200 K with carrier concentration in the low 10^{17} cm^{-3} range, similar to that reported by Analytis et al.[10] We performed four-probe measurements at 10 K, 82 K, and room temperature consecutively (measurement procedure described in the Method). Figure 5b shows the results obtained at T = 10 K less than 18 h after cleavage (with s_{14} = 38.6 μm). On this freshly cleaved surface, we obtain g = 399, which means that the surface conductance is only about 0.25% of the total conductance, consistent with estimate from Analytis et al.[10] where the topological surface contribution was reported to be around 0.1% on Bi_2Se_3 at T = 1.4 K. Thus, the electronic transport is still 3D dominated. The corresponding bulk resistivity is extracted as 2.1 mΩ·cm. The surface resistivity is found to be 218.5 Ω which is subject to a high uncertainty. After measurements at 10 K, the sample was warmed up to 82 K. During this process, the sample was exposed to a pressure in the range of (2—9) × 10^{-9} Torr for about 1 h which was then brought back to about 2×10^{-10} Torr for the measurement. At 82 K on the same sample area and the same probe spacing, we find g = 35 (Figure 5c), indicating a much higher contribution (~2.9%) from the surface to the total conductance. The history of the measurement suggests that the enhanced 2D

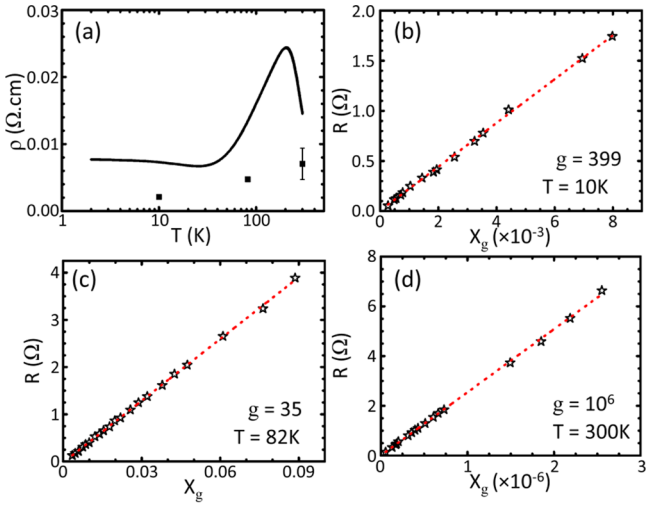

Figure 5. Four-probe transport measurements performed on a Sb-doped Bi_2Se_3 surface at different temperatures. (a) Bulk resistivity of the same sample as a function of the temperature. For comparison, the extracted 3D resistivity values from the four-probe spectroscopy measurements are shown as black squares. (b) T = 10 K (2D + 3D mixture, g = 399). (c) T = 82 K (2D + 3D mixture, g = 35). (d) T = 300 K (pure 3D transport).

contribution may be associated with the additional carriers introduced by the aging effect, similar to the aged Bi_2Te_2Se sample. At room temperature (Figure 5d), no 2D contribution can be detected anymore due to the overwhelming 3D component out of the activated bulk carriers. We also note that the bulk resistivity values (Figure 5a) acquired on the entire sample are higher than those extracted from the local measurements on the surface.

To clearly identify conductance contribution of topological surface states, the effort so far has been focused on reducing the bulk contribution by improving the material quality or decreasing the sample thickness. Our analysis here highlights another aspect. We find that there is a detection window $0.1 < g < 1000$ in order to probe the mixed contributions from the surface and bulk. Since $g = (\rho_{2D}/\rho_{3D})s_{14}$, depending on the ratio of $c = \rho_{2D}/\rho_{3D}$ we can adjust the source probe spacing s_{14} to move g into the detection window, as schematically shown in Figure 6. This reinforces a fundamental rule of the four-probe transport measurement that the detection of a low surface conductance with respect to the bulk (high c) is achievable only at small dimensions[23,24] (low s_{14}) and vice versa. Indeed, in order to measure the small contribution to the transport from the surface, the lateral dimension of the investigated device (sample and probes) must be reduced. Lowering the source probe spacing s_{14} reduces the proportion of the current carried through the bulk (bulk carriers) and increases the measurement sensitivity to the current carried by the surface.

In the past, it has been popular in four-probe measurements to use a probe arrangement with an equidistant probe spacing either in collinear or square configuration and then acquire the resistance as a function of varying probe spacing. Considering a collinear arrangement with an equidistant probe spacing ($s_{ii+1} = d$ and $s_{14} = 3d$), eq 7 becomes

$$R = \rho_{2D} \times \frac{1}{\pi} \ln\left(\frac{g+3}{g+1.5}\right) \quad (11)$$

DOI: 10.1021/acs.nanolett.5b04425
Nano Lett. 2016, 16, 2213−2220

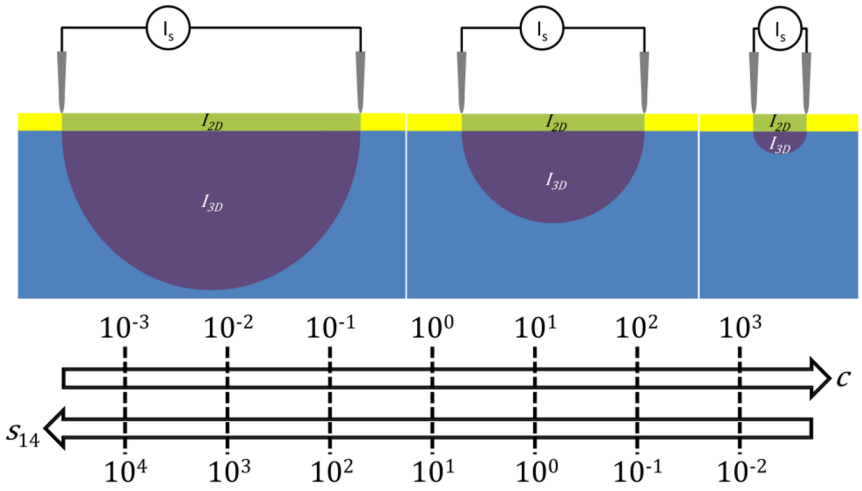

Figure 6. Parameter window for probing different conduction channels. Upper panel: Schematic representation of the contribution of the surface current (I_{2D}, green) and bulk current (I_{3D}, purple) to the total sourced current I_S in function of the source probe spacing. Lower panel: Log scale representation of the relation between the source probe spacing s_{14} and the accurately measurable related c value for $g = c \times s_{14} = 10$.

In the case of a pure 2D system, we have $g = 0$, and this equation gives the well-known result $R = \rho_{2D}(1/\pi)\ \ln(2)$. However, for small but nonzero values of g, with $g = (\rho_{2D}/\rho_{3D})\ s_{14}$, the resistance value obtained from eq 11 may differ by only a few percent even if s_{14} changes by several orders of magnitude. The narrow variation of the measured resistance as a function of the probe spacing can be mistaken as constant (a signature of 2D conduction) within the experimental noise particularly for small values of ρ_{2D} or s_{14}. The same analysis also applies to an equidistant square configuration of probes. This could lead to an erroneous conclusion that the conduction is purely 2D even when there is still a significant contribution from the bulk.

In summary, we report a quantitative measurement of both surface 2D and bulk 3D conductance in topological insulators. The measurement is enabled by a new transport spectroscopy method which considers both the 2D and 3D conduction channels and their interactions. The method addresses the limitation of a widely adopted transport spectroscopy approach in which the two conduction channels are assumed to be "unphysically" decoupled and can be used to understand the myriad of phenomena in 3D TI materials and the 2D to 3D crossover of conductance in other complex systems such as correlated electron systems.[39]

Methods. *Four-Probe Transport Measurements Procedure.* The transport measurements are performed in a cryogenic four-probe scanning tunneling microscope (STM), a characterization platform combining four STM scanners with an in situ scanning electron microscope (SEM) under ultrahigh vacuum (UHV) environment (base pressure ~2 × 10^{-10} Torr).[27] The four STM scanners are independently controllable and the positioning of the tips (electrochemically etched tungsten wire) used as contact probes is controlled under SEM with the precision offered by the STM scanners. The contacts between the tips and the surface are monitored with the STM current preamplifiers. On the surface, the four STM tips are connected in a collinear configuration, the distances s_{ij} between the probes being determined from the SEM images, as schematically shown in Figure 1. For a complete set of measurements, the voltage probes are first connected near the source probes (~2 μm away for $s_{14} \approx 40$ μm) and then moved step by step toward the center of the investigated area, while the positions of the outer source probes are usually fixed.

Special effort has been made to maintain UHV conditions in order to preserve the integrity of the topological surface states.[22] Theoretical calculations showed that the TI surface properties can change when contacting with large metallic contacts leads due to hybridization with the metallic states.[40] In our setup, we use STM tips as in situ electrical contacts, which can keep the influence of the metal on the topological insulator as small as possible due to the reduced contact area compared with the usually applied ex situ contacting methods, like adding Ag paint or sputtered contact pads.

Sample Preparation. Bi_2Se_3 bulk single crystals were synthesized by modified Bridgman method.[18] The as-grown Bi_2Se_3 is *n*-doped with the Fermi level located in the conduction band. The high-quality Bi_2Te_2Se single crystals were synthesized by the Bridgman technique, similar to those previously reported.[32] Sb-doped Bi_2Se_3 crystals are prepared with a Bridgman method as reported by Analytis et al.[10] Briefly, a 3 g boule was made by melting together Bi, Se, and Sb in the molar ratio 52:130:7 at 750 °C for 6 h in a silica tube that had been evacuated and refilled with 1/6 atm argon. The melt was cooled at 1.8 °C/h from 750 to 400 °C, held at this temperature for 100 h, then cooled to room temperature with the furnace power turned off.

AUTHOR INFORMATION

Corresponding Author

*E-mail: apli@ornl.gov.

Notes

The authors declare no competing financial interest.

ACKNOWLEDGMENTS

This research was conducted at the Center for Nanophase Materials Sciences, which is a DOE Office of Science User Facility. MAM acknowledges support for Bi_2Se_3 crystal growth and bulk characterization from the DOE Office of Science, Basic Energy Sciences, Materials Sciences and Engineering Division. The Bi_2Te_2Se crystal growth and characterization at Purdue was supported by DARPA MESO program (Grant

DOI: 10.1021/acs.nanolett.5b04425
Nano Lett. 2016, 16, 2213−2220

N66001-11-1-4107). Authors acknowledge Randall Feenstra for providing the epitaxial graphene for the study.

REFERENCES

(1) Perkins, E.; Barreto, L.; Wells, J.; Hofmann, P. Surface-sensitive conductivity measurement using a micro multi-point probe approach. *Rev. Sci. Instrum.* **2013**, *84*, 033901.
(2) Barreto, L.; Perkins, E.; Johannsen, J.; Ulstrup, S.; Fromm, F.; Raidel, C.; Seyller, T.; Hofmann, P. Detecting the local transport properties and the dimensionality of transport of epitaxial graphene by a multi-point probe approach. *Appl. Phys. Lett.* **2013**, *102*, 033110.
(3) Wells, J. W.; Handrup, K.; Kallehauge, J. F.; Gammelgaard, L.; Bøggild, P.; Balslev, M. B.; Hansen, J. E.; Petersen, P. R. E.; Hofmann, P. The conductivity of Bi(111) investigated with nanoscale four point probes. *J. Appl. Phys.* **2008**, *104*, 053717.
(4) Barreto, L.; Kühnemund, L.; Edler, F.; Tegenkamp, C.; Mi, J.; Bremholm, M.; Iversen, B. B.; Frydendahl, C.; Bianchi, M.; Hofmann, P. Surface-Dominated Transport on a Bulk Topological Insulator. *Nano Lett.* **2014**, *14*, 3755−3760.
(5) Bernevig, B. A.; Hughes, T. L.; Zhang, S.-C. Quantum Spin Hall Effect and Topological Phase Transition in HgTe Quantum Wells. *Science* **2006**, *314*, 1757−1761.
(6) König, M.; Wiedmann, S.; Brüne, C.; Roth, A.; Buhmann, H.; Molenkamp, L. W.; Qi, X.-L.; Zhang, S.-C. Quantum Spin Hall Insulator State in HgTe Quantum Wells. *Science* **2007**, *318*, 766−770.
(7) Chen, Y. L.; Analytis, J. G.; Chu, J.-H.; Liu, Z. K.; Mo, S.-K.; Qi, X. L.; Zhang, H. J.; Lu, D. H.; Dai, X.; Fang, Z.; Zhang, S. C.; Fisher, I. R.; Hussain, Z.; Shen, Z.-X. Experimental Realization of a Three-Dimensional Topological Insulator, Bi_2Te_3. *Science* **2009**, *325*, 178−181.
(8) Hsieh, D.; Xia, Y.; Qian, D.; Wray, L.; Dil, J. H.; Meier, F.; Osterwalder, J.; Patthey, L.; Checkelsky, J. G.; Ong, N. P.; Fedorov, A. V.; Lin, H.; Bansil, A.; Grauer, D.; Hor, Y. S.; Cava, R. J.; Hasan, M. Z. A tunable topological insulator in the spin helical Dirac transport regime. *Nature* **2009**, *460*, 1101−1105.
(9) Bianchi, M.; Guan, D.; Bao, S.; Mi, J.; Iversen, B. B.; King, P. D. C.; Hofmann, P. Coexistence of the topological state and a two-dimensional electron gas on the surface of Bi_2Se_3. *Nat. Commun.* **2010**, *1*, 128.
(10) Analytis, J. G.; McDonald, R. D.; Riggs, S. C.; Chu, J.-H.; Boebinger, G. S.; Fisher, I. R. Two-dimensional surface state in the quantum limit of a topological insulator. *Nat. Phys.* **2010**, *6*, 960−964.
(11) Qu, D.-X.; Hor, Y. S.; Xiong, J.; Cava, R. J.; Ong, N. P. Quantum Oscillations and Hall Anomaly of Surface States in the Topological Insulator Bi_2Te_3. *Science* **2010**, *329*, 821−824.
(12) Jauregui, L. A.; Pettes, M. T.; Rokhinson, L. P.; Shi, L.; Chen, Y. P. Gate Tunable Relativistic Mass and Berry's phase in Topological Insulator Nanoribbon Field Effect Devices. *Sci. Rep.* **2015**, *5*, 8452.
(13) Peng, H.; Lai, K.; Kong, D.; Meister, S.; Chen, Y.; Qi, X.-L.; Zhang, S.-C.; Shen, Z.-X.; Cui, Y. Aharonov-Bohm interference in topological insulator nanoribbons. *Nat. Mater.* **2010**, *9*, 225−229.
(14) Chen, J.; Qin, H. J.; Yang, F.; Liu, J.; Guan, T.; Qu, F. M.; Zhang, G. H.; Shi, J. R.; Xie, X. C.; Yang, C. L.; Wu, K. H.; Li, Y. Q.; Lu, L. Gate-Voltage Control of Chemical Potential and Weak Antilocalization in Bi_2Se_3. *Phys. Rev. Lett.* **2010**, *105*, 176602.
(15) Roushan, P.; Seo, J.; Parker, C. V.; Hor, Y. S.; Hsieh, D.; Qian, D.; Richardella, A.; Hasan, M. Z.; Cava, R. J.; Yazdani, A. Topological surface states protected from backscattering by chiral spin texture. *Nature* **2009**, *460*, 1106−1109.
(16) Zhang, T.; Levy, N.; Ha, J.; Kuk, Y.; Stroscio, J. A. Scanning tunneling microscopy of gate tunable topological insulator Bi_2Se_3 thin films. *Phys. Rev. B: Condens. Matter Mater. Phys.* **2013**, *87*, 115410.
(17) Nurmamat, M.; Krasovskii, E. E.; Kuroda, K.; Ye, M.; Miyamoto, K.; Nakatake, M.; Okuda, T.; Namatame, H.; Taniguchi, M.; Chulkov, E. V.; Kokh, K. A.; Tereshchenko, O. E.; Kimura, A. Unoccupied topological surface state in Bi_2Te_2Se. *Phys. Rev. B: Condens. Matter Mater. Phys.* **2013**, *88*, 081301.
(18) Jia, S.; Ji, H.; Climent-Pascual, E.; Fuccillo, M. K.; Charles, M. E.; Xiong, J.; Ong, N. P.; Cava, R. J. Low-carrier-concentration crystals of the topological insulator Bi_2Te_2Se. *Phys. Rev. B: Condens. Matter Mater. Phys.* **2011**, *84*, 235206.
(19) Mi, J.-L.; Bremholm, M.; Bianchi, M.; Borup, K.; Johnsen, S.; Søndergaard, M.; Guan, D.; Hatch, R. C.; Hofmann, P.; Iversen, B. B. Phase Separation and Bulk p-n Transition in Single Crystals of Bi_2Te_2Se Topological Insulator. *Adv. Mater.* **2013**, *25*, 889−893.
(20) Scanlon, D. O.; King, P. D. C.; Singh, R. P.; de la Torre, A.; Walker, S. M.; Balakrishnan, G.; Baumberger, F.; Catlow, C. R. A. Controlling Bulk Conductivity in Topological Insulators: Key Role of Anti-Site Defects. *Adv. Mater.* **2012**, *24*, 2154−2158.
(21) Zhang, G.; Qin, H.; Chen, J.; He, X.; Lu, L.; Li, Y.; Wu, K. Growth of Topological Insulator Bi_2Se_3 Thin Films on $SrTiO_3$ with Large Tunability in Chemical Potential. *Adv. Funct. Mater.* **2011**, *21*, 2351−2355.
(22) Hoefer, K.; Becker, C.; Rata, D.; Swanson, J.; Thalmeier, P.; Tjeng, L. H. Intrinsic conduction through topological surface states of insulating Bi_2Te_3 epitaxial thin films. *Proc. Natl. Acad. Sci. U. S. A.* **2014**, *111*, 14979−14984.
(23) Hasegawa, S.; Shiraki, I.; Tanabe, F.; Hobara, R.; Kanagawa, T.; Tanikawa, T.; Matsuda, I.; Petersen, C. L.; Hansen, T. M.; Boggild, P.; Grey, F. Electrical conduction through surface superstructures measured by microscopic four-point probes. *Surf. Rev. Lett.* **2003**, *10*, 963−980.
(24) Hasegawa, S.; Grey, F. Electronic transport at semiconductor surfaces - from point-contact transistor to micro-four-point probes. *Surf. Sci.* **2002**, *500*, 84−104.
(25) Tanikawa, T.; Matsuda, I.; Kanagawa, T.; Hasegawa, S. Surface-State Electrical Conductivity at a Metal-Insulator Transition On Silicon. *Phys. Rev. Lett.* **2004**, *93*, 016801.
(26) Tanikawa, T.; Matsuda, I.; Hobara, R.; Hasegawa, S. Variable-Temperature Micro-Four-Point Probe Method for Surface Electrical Conductivity Measurements in Ultrahigh Vacuum. *e-J. Surf. Sci. Nanotechnol.* **2003**, *1*, 50−56.
(27) Gutierrez, H. R.; Perea-Lopez, N.; Elias, A. L.; Berkdemir, A.; Wang, B.; Lv, R.; Lopez-Urias, F.; Crespi, V. H.; Terrones, H.; Terrones, M. Extraordinary Room-Temperature Photoluminescence in Triangular WS2Monolayers. *Nano Lett.* **2013**, *13*, 3447−3454.
(28) Clark, K. W.; Zhang, X. G.; Vlassiouk, I. V.; He, G.; Feenstra, R. M.; Li, A.-P. Spatially Resolved Mapping of Electrical Conductivity across Individual Domain (Grain) Boundaries in Graphene. *ACS Nano* **2013**, *7*, 7956−7966.
(29) Srivastava, L. N.; He, G.; Feenstra, R. M.; Fisher, P. J. Comparison of graphene formation on C-face and Si-face SiC {0001} surfaces. *Phys. Rev. B: Condens. Matter Mater. Phys.* **2010**, *82*, 235406.
(30) Berger, C.; Song, Z.; Li, T.; Li, X.; Ogbazghi, A. Y.; Feng, R.; Dai, Z.; Marchenkov, A. N.; Conrad, E. H.; First, P. N.; de Heer, W. A. Ultrathin Epitaxial Graphite: 2D Electron Gas Properties and a Route toward Graphene-based Nanoelectronics. *J. Phys. Chem. B* **2004**, *108*, 19912−19916.
(31) Ren, Z.; Taskin, A. A.; Sasaki, S.; Segawa, K.; Ando, Y. Large bulk resistivity and surface quantum oscillations in the topological insulator Bi_2Te_2Se. *Phys. Rev. B: Condens. Matter Mater. Phys.* **2010**, *82*, 241306.
(32) Cao, H.; Liu, C.; Tian, J.; Xu, Y.; Miotkowski, I.; Hasan, M. Z.; Chen, Y. P. Controlling and distinguishing electronic transport of topological and trivial surface states in a topological insulator. *arXiv*:1409.3217.
(33) Neupane, M.; Xu, S.-Y.; Wray, L. A.; Petersen, A.; Shankar, R.; Alidoust, N.; Liu, C.; Fedorov, A.; Ji, H.; Allred, J. M.; Hor, Y. S.; Chang, T.-R.; Jeng, H.-T.; Lin, H.; Bansil, A.; Cava, R. J.; Hasan, M. Z. Topological surface states and Dirac point tuning in ternary topological insulators. *Phys. Rev. B: Condens. Matter Mater. Phys.* **2012**, *85*, 235406.
(34) Zhou, B.; Liu, Z. K.; Analytis, J. G.; Igarashi, K.; Mo, S. K.; Lu, D. H.; Moore, R. G.; Fisher, I. R.; Sasagawa, T.; Shen, Z. X.; Hussain, Z.; Chen, Y. L. Controlling the carriers of topological insulators by bulk and surface doping. *Semicond. Sci. Technol.* **2012**, *27*, 124002.

DOI: 10.1021/acs.nanolett.5b04425
Nano Lett. 2016, 16, 2213−2220

(35) Koleini, M.; Frauenheim, T.; Yan, B. Gas Doping on the Topological Insulator Bi2Se3 Surface. *Phys. Rev. Lett.* **2013**, *110*, 016403.
(36) Chen, C.; He, S.; Weng, H.; Zhang, W.; Zhao, L.; Liu, H.; Jia, X.; Mou, D.; Liu, S.; He, J.; Peng, Y.; Feng, Y.; Xie, Z.; Liu, G.; Dong, X.; Zhang, J.; Wang, X.; Peng, Q.; Wang, Z.; Zhang, S.; Yang, F.; Chen, C.; Xu, Z.; Dai, X.; Fang, Z.; Zhou, X. J. Robustness of topological order and formation of quantum well states in topological insulators exposed to ambient environment. *Proc. Natl. Acad. Sci. U. S. A.* **2012**, *109*, 3694−3698.
(37) Checkelsky, J. G.; Hor, Y. S.; Liu, M. H.; Qu, D. X.; Cava, R. J.; Ong, N. P. Quantum Interference in Macroscopic Crystals of Nonmetallic Bi_2Se_3. *Phys. Rev. Lett.* **2009**, *103*, 246601.
(38) Taskin, A. A.; Segawa, K.; Ando, Y. Oscillatory angular dependence of the magnetoresistance in a topological insulator $Bi_{1-x}Sb_x$. *Phys. Rev. B: Condens. Matter Mater. Phys.* **2010**, *82*, 121302.
(39) Kim, T.-H.; Angst, M.; Hu, B.; Jin, R.; Zhang, X.-G.; Wendelken, J. F.; Plummer, E. W.; Li, A.-P. Imaging and manipulation of the competing electronic phases near the Mott metal-insulator transition. *Proc. Natl. Acad. Sci. U. S. A.* **2010**, *107*, 5272−5275.
(40) Culcer, D.; Hwang, E. H.; Stanescu, T. D.; Das Sarma, S. Two-dimensional surface charge transport in topological insulators. *Phys. Rev. B: Condens. Matter Mater. Phys.* **2010**, *82*, 155457.

DOI: 10.1021/acs.nanolett.5b04425
Nano Lett. 2016, 16, 2213−2220